Cement and Concrete Research 142 (2021) 106381

Contents lists available at ScienceDirect

Cement and Concrete Research

journal homepage: www.elsevier.com/locate/cemconres

NO_x sequestration by calcium aluminate cementitious materials

Qingxu Jin [a], Sarah L. Hordern [a,b], Yuanzhi Tang [a,c], Kimberly E. Kurtis [a,*]

[a] School of Civil and Environmental Engineering, Georgia Institute of Technology, Atlanta, GA 30332, USA
[b] Department of Civil, Architectural and Environmental Engineering, Austin, The University of Texas at Austin, Austin, TX 78712, USA
[c] School of Earth and Atmospheric Sciences, Georgia Institute of Technology, Atlanta, GA 30332, USA

ARTICLE INFO

Keywords:
Calcium aluminate cement
TiO_2 photocatalysts
NO_x sequestration
Nitrite/nitrate binding
Surface area

ABSTRACT

This study quantifies NO_x uptake efficiency and explores NO_x binding mechanisms in calcium aluminate cementitious (CAC) materials. Comparison between unmodified and TiO_2-modified CAC separates intrinsic NO_x binding mechanisms from those related to photocatalysis. Attributed to surface-related heterogeneous reactions, the NO_x binding occurs in unmodified CAC at nitrite-to-nitrate ratio of 1: 1.3 and can be increased with surface area. The photocatalytic reactions in TiO_2-modified CAC increase NO_x uptake, and ~50% of converted NO_x resists releasing back into the environment via dissolution. Compared to previously studied ordinary portland cement (OPC) materials, CAC increases NO_x uptake capacity and demonstrates a more permanent NO_x binding, potentially mitigating concerns related to the release of previously bound N-species in OPC. Examination of the interaction between NO_x and a synthetic pure aluminum-bearing phase shows that the permanent NO_x uptake in CAC could be largely attributed to the chemical binding of converted NO_x within aluminum-bearing phases.

1. Introduction

Nitrogen oxides (NO_x) are hazardous and highly reactive air pollutants, causing a wide variety of health and environmental problems such as impairment of the human respiratory and visual systems and the formation of tropospheric ozone and urban smog [1]. Although efforts have been made to reduce concentrations of NO_x in the atmospheric environment, urban NO_x levels are still increasing due to lack of air flow, increasing use of cars with small combustion engines, and increased industrial zones [2]. As a promising pathway for sequestering atmospheric NO_x, titanium dioxide (TiO_2) photocatalysts have been proposed to be used in combination with cement-based materials [3]. In the presence of water, oxygen, and ultraviolet (UV) light, TiO_2 can effectively convert atmospheric NO_x into nitrite (NO_2^-) and nitrate (NO_3^-) [4,5], which can be bound within the complex structure of cementitious materials [6,7].

TiO_2-modified cementitious materials have been used in both exterior and interior applications, such as building facades, exterior tiles, roofs, concrete pavements, tunnels, and interior walls [8]. The global market for photocatalysts has increased exponentially in recent decades, was worth 2.1 billion U.S. dollars in 2017, and is expected to increase to 5.3 billion U.S. dollars by 2025 [9]. One third of this photocatalytic market is attributed to applications of air purification [9]. In Japan, the sale of photocatalytic cementitious materials accounts for more than 60% of their total photocatalytic market [10].

The large potential of TiO_2-modified cementitious materials has prompted extensive study, including the design of various TiO_2 photocatalysts [11–13], as well as the exploration of the fundamentals of photocatalytic reactions [8,14,15] and the surface and microstructural features that affect the photocatalytic efficiency of NO_x sequestration [6,7]. Recently, studies have quantified the photocatalytic efficiency in OPC-based cementitious materials, with measurements of NO_2^- and NO_3^- produced by photocatalysis on the surfaces and the efficiency with which those ions are bound within the cementitious material as a function of the material's microstructural features [6]. Three types of binding in OPC-based materials have been theorized – I) the adsorption of NO_2^- and NO_3^- on the surface of cement hydrates such as C-S-H[1] [6,8,16], II) the reaction of these ions with hydroxyls in materials' alkaline environment [17,18], and III) substitution of these ions into aluminum-bearing hydrates (e.g., AFm) through anion substitution process [19,20]. Moreover, studies have shown when N-substituted phases interact with ingressing Cl^- ions, ion exchange reactions can occur, releasing nitrite and nitrate ions into the pore solution [21,22]. The release of nitrate and nitrite into the pore solution can enhance

* Corresponding author.
E-mail address: kkurtis@gatech.edu (K.E. Kurtis).

[1] Standard cement chemistry abbreviations are used in this paper: C=CaO, S=SiO_2, A = Al_2O_3, and H=H_2O.

https://doi.org/10.1016/j.cemconres.2021.106381
Received 29 September 2020; Received in revised form 7 January 2021; Accepted 24 January 2021
Available online 9 February 2021

corrosion resistance, relying on chemical interactions at the steel/concrete interface currently associated with nitrate- and/or nitrite-containing corrosion-inhibiting admixtures [23,24].

While portland cement is, by far, the most widely used cement, it may not be the most advantageous substrate cement for applications intended to bind NO_x. One of the major drawbacks is that the binding of photocatalytic-converted NO_2^- and NO_3^- to OPC substrates is impermanent [6,7]. For example, NO_2^- and NO_3^- held within the OPC structure can be extracted by water [6,7]; such leaching can affect groundwater, aquatic and forest systems, and agriculture [25]. In addition, certain amounts of NO_2, which are produced in the photocatalytic process ($HNO_2 + OH^\bullet \rightarrow NO_2 + H_2O$), can be released back into the atmosphere [26,27]. Acid formation during the photocatalytic reactions ($NO + OH^\bullet \rightarrow NO_2^- + H^+$ and $NO_2 + OH^\bullet \rightarrow NO_3^- + H^+$) is considered another drawback since decomposition of hydrated cement phases, such as C-S-H [28], can compromise surface integrity, strength, and overall durability [29]. These concerns suggest that the binding of NO_x within OPC could be transient and even potentially damaging to the substrate and cement-based composite performance.

Therefore, alternative cementitious systems with greater NO_x binding capacity, more permanent NO_x binding capacity and greater durability through interactions with NO_x, particularly to acids that could be formed, should be explored. Calcium aluminate cements (CACs) have been considered a potential candidate [21,22,30] since they are widely available and possess enhanced acid resistance compared to OPC [31,32], which could potentially offer an advantage in case that nitric acid is formed during photocatalytic reactions [29]. The primary component in CAC is monocalcium aluminate (CA), and their hydration products are aluminum-bearing phases. Prior studies on OPC [19,20] and aluminum-rich geopolymers [23,24] have shown the importance of aluminum-bearing phases in chemically binding NO_2^- and NO_3^- in those materials. A previous study has demonstrated the photocatalytic NO_x binding by TiO_2-modified CAC [30]. However, the binding mechanism in CAC materials has not been explored and the inherent NO_x sequestration capacity in CAC materials has not been previously quantified.

Going beyond preliminary 'proof-of-concept' demonstration of NO_x capture by TiO_2-modified CAC materials, this study aims to quantify photocatalytic efficiency and to bring new understanding of binding capacity and mechanisms by combining standardized NO_x degradation experiments on CAC pastes with photocatalysts, characterization of the substrate materials, and targeted examination of a key aluminum-bearing phase. Long-term efficiency in ordinary (unmodified) and TiO_2-modified CAC is examined by performing multiple UV-light "on-off" cycles to replicate diurnal exposure conditions. The effects of TiO_2 nanoparticles on the CAC composites, including microstructural properties and TiO_2 dispersion are analyzed using N_2 adsorption and desorption isotherms, scanning electron microscopy (SEM), and X-ray diffraction (XRD). To quantitatively assess the NO_x binding mechanisms in CAC materials, a combination of wet chemical extraction, UV–visible spectrophotometry, and ion chromatography is employed. The NO_x uptake capacities of both unmodified and TiO_2-modified CAC are quantified and the results are compared with our previously examined OPC-based cementitious materials [6]. In addition, to examine the interaction of NO_x with aluminum-bearing phase, studies are performed on an AFm (Al_2O_3-Fe_2O_3-monophase) phase, which provides a better understanding on the mechanisms of NO_x binding in aluminum-rich cementitious materials.

2. Materials and methods

2.1. Materials

Pastes were prepared from calcium aluminate cement (CAC) (Kerneos, Chesapeake, VA, USA) and deionized water (18.2 MΩ·cm) with 0% (control) and 5% (by mass) cement replacement with photocatalytic TiO_2 nanoparticles (KRONOClean® 7050, Kronos Worldwide, Dallas, TX, USA). The water-to-solid ratio was kept at 0.40 by mass. The chemical compositions of the CAC and TiO_2 photocatalyst, obtained by X-ray fluorescence (XRF) spectrometry, are given in Tables 1 and 2, respectively. Other characteristics of the TiO_2 photocatalyst provided by the manufacturer are also provided in Table 2. The photocatalytic performance of TiO_2 nanoparticles is optimized under UV irradiance of 10 W m^{-2}.

Two types of samples were prepared for control and 5% TiO_2-modified CAC – plate and granular samples – for different purposes and characterization tests. The plate samples were prepared based on ISO 22197 [33] and JIS R 1701 Standards [34] and used to study the NO_x degradation of TiO_2-modified CAC. TiO_2 photocatalysts were first added to deionized water, and the suspension was mixed for 1 min using a handheld electric mixer to facilitate particle dispersion. Cement was then added to the TiO_2 suspension and mixed for 2 min. Plate samples of $50 \times 50 \times 10$ mm^3 (width × length × height) were cast in polyethylene plastic molds and stored at 23 ± 2 °C under polyethylene sheeting. After 24 h, the plates were removed from the molds and subsequently cured in limewater in a sealed container at 23 ± 2 °C for 28 days. After curing, samples were stored in double sealed plastic bags prior to characterization tests to avoid carbonation or drying.

The preparation of granular samples was adopted from ref [6]. The use of granular samples not only facilitates the examination of the binding mechanism(s) and NO_x uptake capacity of CAC samples due to the greater surface area for reaction, but also allows for direct comparison with OPC-based samples that were prepared and tested in the same manner [6]. The samples were produced by hand-crushing one of the plate samples and sieved to particle sizes of 0.6–1 mm. Granular samples were stored in the same manner as plate samples before characterizations.

To demonstrate the interaction of NO_x with aluminum-bearing phase, AFm-SO_4 (Al_2O_3-Fe_2O_3-monosulfate) was synthesized according to the protocol developed by Matschei [35]. This phase was selected because it is structurally similar to C_2AH_8 phase, which is one major phase in hydrated CAC [36]. Also, it can be produced reliably in the laboratory and remains relatively stable under lab conditions. It was prepared by mixing C_3A (Mineral Research Processing, Meyzieu, France) and $CaSO_4$ in a 1:1 molar ratio in boiling deionized water with a water/solid mass ratio of around 20. The slurry was then stirred at 85 °C for two weeks in a sealed polytetrafluoroethylene (PTFE) bottle prior to filtration with Whatman grade 1 filter paper and vacuum-drying. XRD analysis (Section 2.2.4) confirmed the phase purity of >99%. The sample was then stored in a doubly sealed HDPE bottle at 23 ± 2 °C before characterizations.

2.2. Characterization

2.2.1. Thermogravimetric analysis

To identify the hydration phases and quantify the bound water for both unmodified and TiO_2-modified CAC samples, thermogravimetric analysis (TGA) was carried out using Hitachi TG/DTA 7300. Approximately 60 mg of cementitious pastes were ground to a particle size of <74 μm (No.200 sieve) and placed in a 70 μL platinum crucible. Samples were dried at 40 °C for 15 min or until reaching constant mass if mass had not stabilized within 15 min. The sample was then heated from 40 °C to 1000 °C at a rate of 10 °C min^{-1}. Nitrogen was used to purge at a flow rate of 100 mL min^{-1}.

2.2.2. N_2 adsorption and desorption isotherms

The specific surface area (SSA) and pore size distribution (PSD) of the granular samples were measured by Brunauer-Emmett-Teller (BET) N_2 adsorption and desorption isotherms [37]. Tests were conducted on ~2 g of granular samples in a gas analyzer (Micromeritics ASAP 2420) over a pressure range of 0.01 to 0.99 atm. The samples were degassed at 1.33 kPa pressure for 12 h prior to the analysis. Although a previous study has shown that surface area measurements vary with techniques and sample

Table 1
Composition (% by mass) and loss on ignition (LOI) of calcium aluminate cement.

SiO_2	Al_2O_3	Fe_2O_3	CaO	MgO	SO_3	Na_2O	LOI	CA	CA_2	C_2AS	$C_{12}A_7$
5.5	45.2	6.9	37.7	0.2	0.1	0.3	1.9	57.0	8.6	16.2	1.5

Table 2
Composition (% by mass) and characteristics of TiO_2 photocatalyst.

TiO_2	Al_2O_3	SiO_2	SO_3	Phase	Bulk density	Crystallite size	Specific surface area
92.3	1.0	3.7	2.0	Anatase	300 g L^{-1}	~15 nm	>225 m^2 g^{-1}

preparation methods [38], BET adsorption-desorption isotherms are commonly used for detecting the relevant microstructural features and facilitating semiquantitative comparisons among different cementitious materials [6,39,40]. In this study, sample preparation was performed through a procedure consistent as ref [6,39,41], in order to facilitate comparison between samples.

2.2.3. Scanning electron microscopy analysis

To investigate the dispersion of TiO_2 nanoparticles, SEM and energy dispersive X-ray spectroscopy (EDS) analyses were performed using a JSM-7600F Schottky Field Emission Scanning Electron Microscope (JEOL, Tokyo, Japan). After curing, a thin sliced specimen was impregnated with low-viscosity epoxy resin, polished, and carbon-coated for better surface conductivity prior to imaging.

2.2.4. X-ray diffraction

XRD was performed on the synthetic AFm-SO_4 phase before and after NO_x exposure to identify changes in mineralogy. Approximately 0.2 g of finely ground powders were packed into a sample holder, and the measurements were taken on a PANalytical Empyrean X-ray diffractometer (Malvern Panalytical Ltd., Malvern, United Kingdom) with Cu-Kα radiation (λ = 1.54 Å) at 45 kV and 40 mA. Scans were performed at 5–45° 2θ using a PIXcel3D detector.

2.2.5. NO_x degradation

NO_x degradation was performed following procedures in the ISO 22197 [33] and JIS R 1701 Standards [34], and test setup is shown in Fig. 1. For plate samples, a sealed reaction chamber with a prismatic cross-section and borosilicate glass cover was constructed, as shown in Fig. 1(b). Three identical plates with a total area of 7500 mm^2 were placed in the reaction chamber for each composition (control or 5% TiO_2-modified CAC). To investigate the long-term photocatalytic efficiency, the plate samples were subjected to three consecutive UV light "on-off" cycles to replicate diurnal exposure conditions. For each cycle, the reaction chamber was pumped with NO_x gas, which was prepared by mixing 1000 ppb nitric oxide in ultrapure dry air at a constant flow rate of 1 L min^{-1} [33,34]. The test was conducted at 23 ± 2 °C and 50 ± 5% relative humidity. The sample-loaded reaction chamber was placed under two UV fluorescent lamps of 40 W with peak emission of 365 nm and UV irradiance of 10 W m^{-2} (Actinic BL TL 40W/10 SLV, Philips Lighting). To achieve an optimal photocatalytic performance, the UV intensity at the sample surface was maintained at 10 W m^{-2} by adjusting the distance between the UV light source and the samples. The initial gas concentration was kept at 1000 ppb before turning on the UV light. After ~1 h, the gas concentration stabilized and UV light exposure started and continued for 5 h. The gas concentration was allowed to re-stabilize for another hour after the UV light was turned off. A chemiluminescent NO/NO_2/NO_x analyzer (Model 200A, Teledyne API, San Diego, CA, USA)

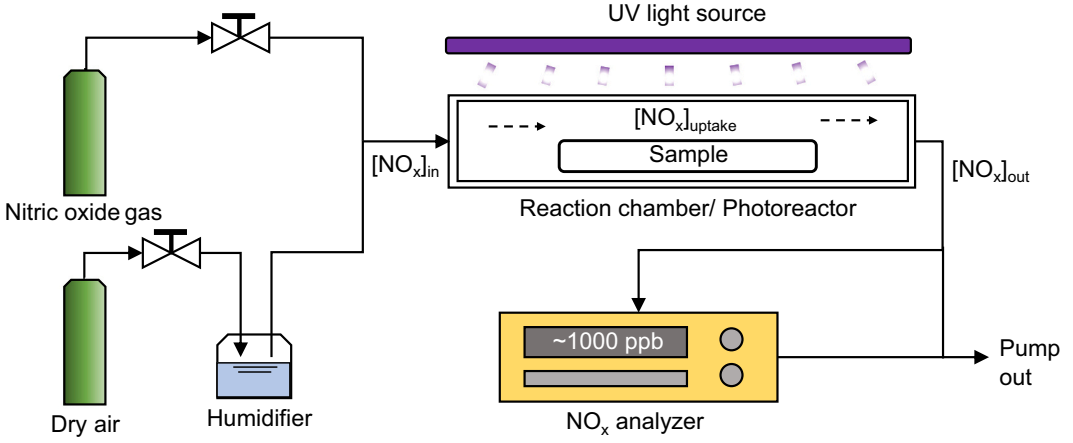

b) Reaction chamber for plate samples

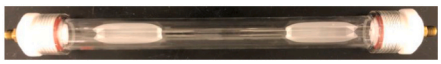

c) Photoreactor for crushed samples

Fig. 1. Experimental setup for NO_x degradation.

was used to measure the gas concentration. The test setup was covered by a black light-blocking canvas to prevent ambient light from affecting the reaction.

Each cycle ended when gas concentration re-stabilized and was followed by 12-hour breaks, during which the samples were not tested or subjected to any surface treatment (e.g., washing the NO_x exposed sample surfaces). Although previous studies [7] have indicated that such treatment could wash the photocatalytically converted N-species away from the surface and reinstate its photocatalytic efficiency, such treatment could also alter the microstructural properties of the sample surface and invalidate the comparison of photocatalytic efficiencies between two cycles. Therefore, to avoid alteration of the sample, no surface treatment was performed after each cycle of exposure in this study.

For granular samples, a sealed tubular borosilicate photoreactor was used with both ends sealed with a filter and screw cap, as shown in Fig. 1 (c). Two grams of the granular samples were placed in two weighing boats rested on the bottom of the reactor. The position of the photoreactor was adjusted to ensure the same UV intensity required by the standards. The same test conditions and procedures were employed for granular samples, except that only one cycle was performed to compare with the previously examined OPC-based samples [6]. At the end of the NO_x photodegradation test, the sample was removed from the photoreactor and stored in double sealed plastic bags with light-blocking foil and was subjected to wet chemical extraction for NO_2^- and NO_3^- measurements within 24 h. The same test setup, conditions, and procedures were also used in AFm-SO_4 phase, except no UV exposure is needed since the phase is directly exposed to NO_x without the addition of TiO_2.

To examine the individual and combined effects of NO_x exposure, UV exposure, and TiO_2 doping, both the unmodified CAC group (denoted as 'CAC') and the 5% TiO_2-modified group (denoted as 'CAC5T') were subjected to three exposure conditions: 1) without NO_x or UV exposure (control); 2) with NO_x but without UV exposure, as denoted as 'N'; and 3) with both NO_x and UV exposures, as denoted as 'NV'. For example, TiO_2-modifed CAC sample subjected to exposure Condition 3 is denoted as 'CAC5T-NV'. The samples subjected to condition 3 were exposed to both NO_x and UV for five hours plus a one-hour stabilization at beginning and another hour for re-stabilization at the end (as described above). To ensure a same period of NO_x exposure as Condition 3, the samples subjected to Condition 2 were exposed to NO_x for a total of seven-hour period without UV exposure, both the unmodified CAC ('CAC') and the 5% TiO_2-modifed CAC ('CAC5T') granular samples.

2.2.6. NO_2^- and NO_3^- measurements

Granular samples were subjected to wet chemical extraction after the NO_x photodegradation test, using the methods previously described in ref [6]. Reacted samples were suspended in anoxic deionized water that was purged by N_2 gas for 48 h. A solid-to-liquid ratio of 0.1 g in 40 mL deionized water was used [6]. This extraction was conducted in aluminum foil-wrapped centrifuge tubes to prevent further photo-induced reactions. After the extraction, the suspension was filtered through a 0.45 μm syringe filter. The filtrate was then analyzed for nitrite and nitrate concentrations. Nitrite concentration was determined using a colorimetric assay kit (Roche, Sigma Aldrich, St. Louis, MO, USA) and measured at 540 nm on a UV–vis spectrometer (Cary 60, Agilent, Santa Clara, CA, USA). Nitrate concentration was determined using ion chromatography (Dionex, Sunnyvale, CA, USA). The ion chromatograph is equipped with an Ionpac® AS14A column (4 × 250 mm) combined with an Ionpac® AG14A guard column (4 × 50 mm), and a Dionex ED40 electrochemical detector. The mobile phase contained a mixture of 8 mM Na_2CO_3 and 1 mM $NaHCO_3$, and the flow rate was 0.8 mL min^{-1}.

2.3. Methodology

2.3.1. Quantification of photocatalytic performance

Through NO_x degradation tests, both photocatalytic efficiency and NO_x uptake can be measured. The photocatalytic efficiency (η_{NOx}) is estimated by comparing the reduction of NO_x concentration to the inlet NO_x concentration [16], which is expressed in Eq. (1).

$$\eta_{NO_x} = \frac{C_{[NO_x]_{in}} - C_{[NO_x]_{out}}}{C_{[NO_x]_{in}}} \times 100\% \quad (1)$$

where η_{NOx} is the photodegradation efficiency (%), $C_{[NOx]in}$ is the inlet concentration of NO_x (ppb), and $C_{[NOx]out}$ is the outlet concentration of NO_x (ppb).

The NO_x degradation capacity that is normalized by sample surface area (S_{NOx}) can be calculated by Eqs. (2) and (3) and in units of mmol m^{-2}. The N mass of NO_x uptake (m_N) through photocatalytic reactions is normalized by sample mass and can be quantified by Eqs. (2) and (4) [6], with the units of mg N per kg solid (denoted as mg kg^{-1} for simplicity).

$$Q_{NO_x} = \frac{f}{V}\int_0^T \left(C_{[NO_x]_{in}} - C_{[NO_x]_{out}}\right)dt \quad (2)$$

$$S_{NO_x} = \frac{Q_{NO_x}}{A} \quad (3)$$

$$m_N = \frac{Q_{NO_x} \times M_N}{m_S} \quad (4)$$

where Q_{NOx} is the NO_x uptake that is measured by the NO_x analyzer (mol), t is the duration of NO_x absorption (min), T is the total duration of the UV-light exposure (300 min), f is the flow rate of NO_x at 23 °C and 1.01 kPa (1 L min^{-1}), V is the volume of 1 mole ideal gas at 23 °C and 1.01 kPa (24.3 L), S_{NOx} is the uptake capacity that is normalized by the UV-exposed surface area (A) of tested plate samples (mmol m^{-2}), m_N is the nitrogen mass of NO_x uptake (mg kg^{-1}), M_N is the molar mass of nitrogen (14 g mol^{-1}) and m_S is the sample mass (kg). The result is then compared with the total nitrogen mass from the NO_2^- (m_N') and NO_3^- (m_N'') measurements, as shown in the following section.

2.3.2. Quantification of NO_2^- and NO_3^- formation

The N mass from nitrite and nitrate measurements is determined by Eqs. (5)–(8) [6].

$$m_{NO_2^-} = C_{NO_2^-} \times DF \quad (5)$$

$$m_{NO_3^-} = C_{NO_3^-} \times DF \quad (6)$$

$$m_N' = m_{NO_2^-} \times \frac{M_N}{M_{NO_2^-}} \quad (7)$$

$$m_N'' = m_{NO_3^-} \times \frac{M_N}{M_{NO_3^-}} \quad (8)$$

where m_{NO2^-} is the mass of nitrite (mg kg^{-1}), m_{NO3^-} is the mass of nitrate (mg kg^{-1}), C_{NO2^-} is the concentration of nitrite measured by UV–vis spectrometer (ppm), C_{NO2^-} is the concentration of nitrate measured by ion chromatography (ppm), DF is the dilution factor used for wet chemical extraction (400), m_N' is the mass of nitrogen from nitrite (mg kg^{-1}), m_N'' is the mass of nitrogen from nitrate (mg kg^{-1}), M_{NO2^-} is the molar mass of nitrite (46 g mol^{-1}), and M_{NO3^-} is the molar mass of nitrate (62 g mol^{-1}).

3. Results and discussion

The effects of TiO_2 nanoparticles on the composition and microstructural properties of CAC pastes are determined by using TGA and N_2

adsorption and desorption isotherms. Two sample geometries are prepared to examine the material's photocatalytic performance: plate samples to examine photocatalytic efficiency, as well as granular samples to quantify NO_x uptake capacity and explore binding mechanisms and to allow for a direct comparison with OPC-based samples that were prepared and tested in the same manner. N-species that are physically bound with hydrated cementitious phases are quantified using a combination of wet chemical extraction, UV-vis spectrophotometry, and ion chromatography. The total NO_x uptake is estimated by combining the results from surface-related heterogeneous reactions and/or photocatalytic reactions. The presence of chemically bound N-species is then estimated by the difference between the total NO_x uptake and that which is physically bound.

3.1. Composition, nano-TiO_2 dispersion, and microstructure

The phase composition of both unmodified CAC paste (CAC) and TiO_2-modified CAC paste (CAC5T) after 28 days of hydration can be identified by TGA (Fig. 2), where the mass losses indicate the decomposition of different phases. The metastable phases of CAH_{10} and C_2AH_8 are identified at temperature of 120 °C and 150 °C, respectively, while stable phases of AH_3 and C_3AH_6 are identified at temperature of 270 °C, and 320 °C, respectively [42]. The TGA results show lesser amounts of hydration products formed in TiO_2-modified samples, likely due to the dilution of the cement with non-hydraulic titania [30]. SEM analysis (Fig. 3) shows well distributed TiO_2 particles within the hydrated CAC sample. The images also show these TiO_2 particles are agglomerates in the range from 1 to 2 μm in diameter.

The measured SSA are 16.68 ± 0.29 $m^2\ g^{-1}$ for CAC and 21.33 ± 0.35 $m^2\ g^{-1}$ for CAC5T after 28 days of hydration. The SSA is increased in CAC5T samples by 27%, which is in the range expected based on the SSA of the material's components. The PSD profiles of both CAC and CAC5T samples are shown in Fig. 4, with a larger number of small pores (<10 nm) observed in CAC5T. Since the amount of hydration products in CAC5T is in fact lower than CAC (Fig. 2), the higher SSA and greater amount of micropores observed in well-hydrated CAC pastes should be mainly attributed to the inclusion of TiO_2 nanoparticles, which intrinsically exhibit high SSA (Table 2).

3.2. Photocatalytic performance

Fig. 5 shows the long-term photocatalytic performance of TiO_2-modified CAC plate samples that are exposed to NO_x and UV (CAC5T-NV) for three consecutive UV "on-off" cycles (the detailed test arrangement can be referred to Section 2.2.5). With a constant NO_x concentration before the UV light was illuminated, an almost

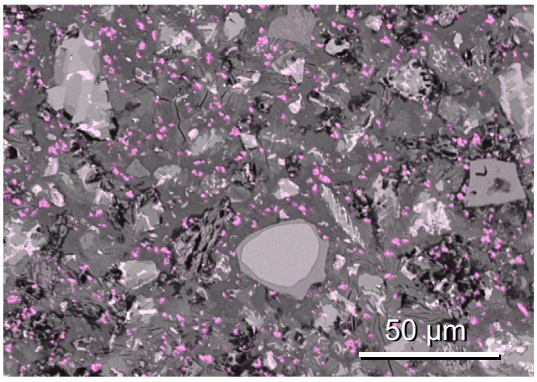

Fig. 3. SEM analysis of TiO_2-modfied CAC (CAC5T) sample with TiO_2 highlighted in pink. (For interpretation of the references to color in this figure, the reader is referred to the web version of this article.)

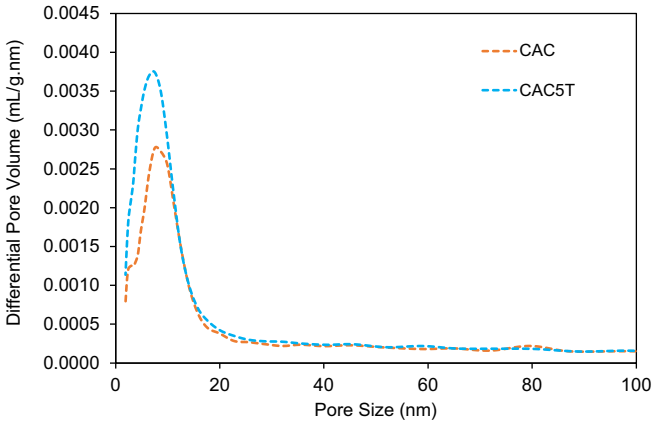

Fig. 4. Pore size distribution of unmodified CAC (CAC) and 5% TiO_2-modfied CAC (CAC5T) samples after 28 days of hydration. (For interpretation of the references to color in this figure legend, the reader is referred to the web version of this article.)

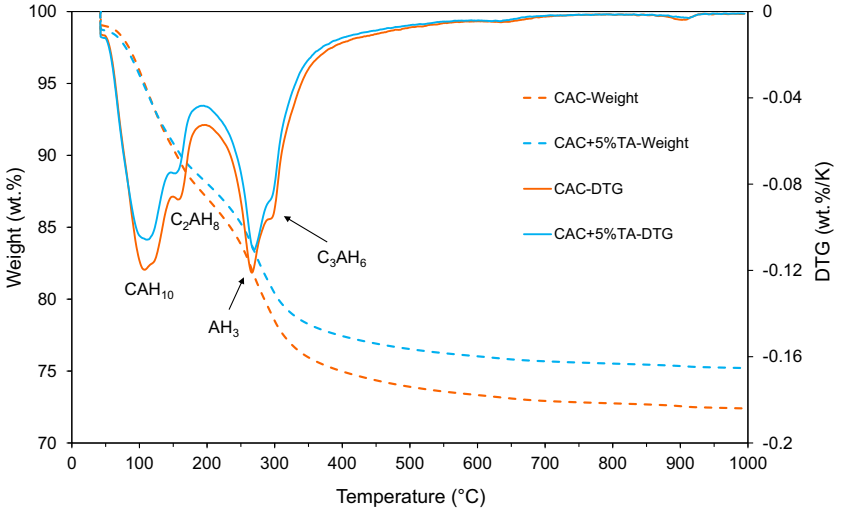

Fig. 2. TGA results of unmodified CAC (CAC) and 5% TiO_2-modfied CAC (CAC5T) samples after 28 days of hydration. (For interpretation of the references to color in this figure legend, the reader is referred to the web version of this article.)

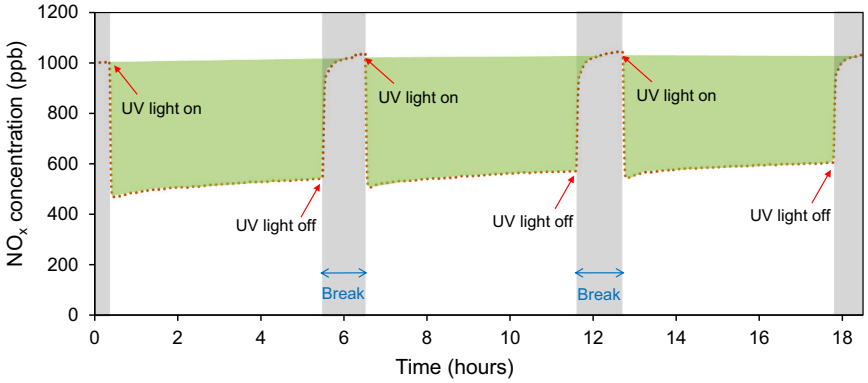

Fig. 5. Photocatalytic performance of plate TiO_2-modified CAC samples that are exposed to NO_x and UV light for three consecutive UV "on-off" cycles.

instantaneous drop of NO_x concentration occurred upon initial UV illumination. The magnitude of the initial drop of TiO_2-modified CAC samples are similar to the CAC samples tested by Pérez-nicolás et al. [30]. However, only a short-term photocatalytic efficiency (30 min) was examined in their study. To show long-term photocatalytic performance, this study examines the NO_x degradation throughout a 5-hour test period during each cycle. This subsequent decrease over the 5-hour period in CAC samples was also observed in TiO_2-modified OPC samples [6,15,43], which were tested under similar conditions. When the UV light was off, the NO_x concentration recovered to its initial level. This phenomenon then occurred repeatedly in the second and third UV light "on-off" cycles.

Table 3 lists the initial and end NO_x concentrations for each cycle, which correspond with the results of NO_x degradation shown in Fig. 5. The initial concentration is the measured NO_x level right after the UV light is on and the end concentration right before the UV light is off. The photocatalytic efficiency (η_{NOx}) at the initial and the end of each cycle is determined by Eq. (1). The highest η_{NOx} of 53% occurred at the initial exposure of the first cycle; it then decreased throughout the 5-hour test period to 46%. When the second cycle began after a 12-hour break from UV exposure, η_{NOx} started at 49% and decreased to 43%, and the η_{NOx} of third cycle decreased from 46% to 40%. Comparing the end concentration of 1st cycle to the initial concentration of 2nd cycle, a small but consistent fraction of the η_{NOx} was recovered (about 3%), and the same restoration phenomenon was also observed between 2nd and 3rd cycles. This restoration phenomenon between cycles, where the test was paused, indicates that a small fraction of NO_x binding with CAC samples is transient and should be taken into consideration for estimating the material's NO_x binding capacity. However, the underlying mechanisms of such restoration phenomenon require further investigations.

The results from Fig. 5 and Table 3 shows a decreasing trend of long-term photocatalytic efficiency over time and with increasing cycles, which implies that the NO_x uptake for TiO_2-modified CAC could reach a limit over time. In addition, this decreasing trend also affects the NO_x degradation capacity (S_{NOx}), which can be estimated using Eqs. (2) and (3). The NO_x uptake capacity for each cycle is also included in Table 3, and it decreases from 800 mmol m^{-2} in the first cycle to 710 mmol m^{-2} in the third cycle. Similar phenomenon was observed in OPC-based plate samples [44–46], where both photocatalytic efficiency and NO_x degradation capacity decrease over time. Recall that no surface treatment (e.g., washing the exposed sample surface) was performed between UV-exposure cycles, to avoid alteration of the sample surface. The impact of washing, as would be experienced during rain, on photocatalytic efficiency deserves further investigation.

Table 3
NO_x concentration ($C_{[NOx]}$) and NO_x uptake capacity (S_{NOx}) of TiO_2-modified CAC plate samples that exposed to NO_x and three consecutive UV light "on-off" cycles. The detailed NO_x degradation can be referred to Fig. 5 and the exposure arrangement can be referred to Section 2.2.5. The NO_x concentration prior to the illumination of UV light is 1000 ppb, the initial concentration is the NO_x level right after UV light is on and the end concentration is right before the UV light is off. The unit of $C_{[NOx]}$ is ppb and the unit of S_{NOx} is mmol m^{-2}.

	1st cycle		2nd cycle		3rd cycle	
	Initial	End	Initial	End	Initial	End
$C_{[NOx]}$ (ppb)	470	540	510	570	540	600
S_{NOx} (mmol m^{-2})	800		760		710	

3.3. Quantification of NO_x uptake

3.3.1. NO_x uptake through photocatalytic reactions

The NO_x degradation achieved by granular TiO_2-modified CAC samples that are exposed to NO_x and UV (CAC5T-NV) is illustrated in Fig. 6. As with the plate samples, an instantaneous drop of NO_x concentration occurred upon initial UV illumination and the photocatalytic efficiency decreased during the test period. When the UV light was turned off, the NO_x concentration recovered to the initial level. The trends of NO_x degradation in the plate and granular samples are essentially the same. The N mass of NO_x uptake (m_N) through photocatalytic reactions, which is represented by the shaded area in Fig. 6 and normalized by sample mass, can be determined by Eqs. (2) and (4). The result is 28.4 ± 0.63 mg N per kg solid (denoted as mg kg^{-1}).

The N mass of NO_x uptake for plate samples is also calculated and normalized by sample mass for the sake of comparison in this study. For the plate samples, the result is 1.58 ± 0.09 mg kg^{-1}, which is significantly lower than granular samples. This result is expected since the UV-exposed surface area per unit mass is increased when the plate sample is crushed into granular samples, and the increase in surface area in turn increases the NO_x binding potential of granular samples. As discussed in

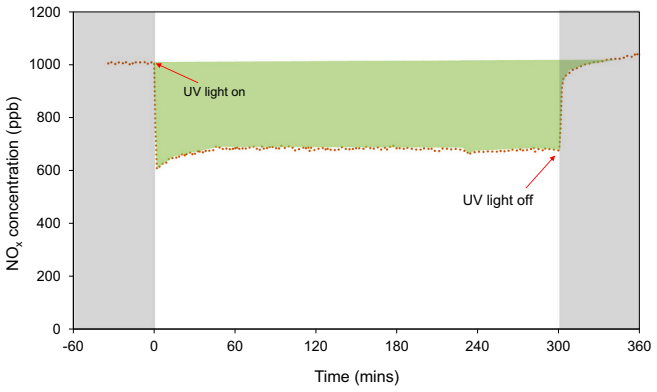

Fig. 6. Photocatalytic performance of granular TiO_2-modified CAC samples that are exposed to NO_x and UV light.

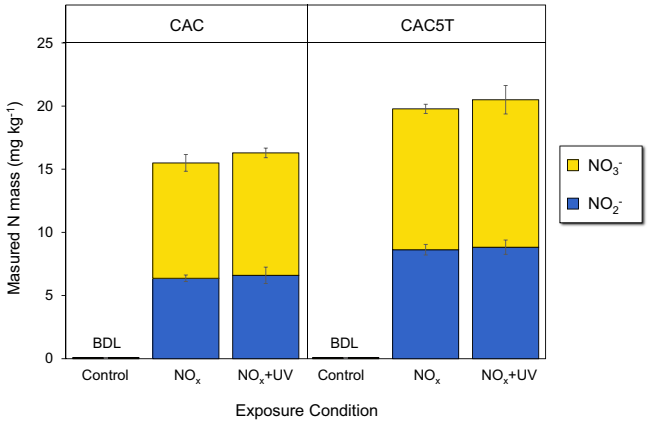

Fig. 7. N mass, as nitrite (NO_2^-, in blue) or nitrate (NO_3^-, in yellow) normalized by sample mass (Section 2.3.2) for both the unmodified CAC ('CAC') and the 5% TiO_2-modifed CAC ('CAC5T') granular samples. Both samples were subjected to each of three exposure conditions: 1) without NO_x or UV exposure (control); 2) with NO_x but without UV exposure; and 3) with both NO_x and UV exposures. BDL: below detection limit. (For interpretation of the references to color in this figure legend, the reader is referred to the web version of this article.)

Section 2.1 and shown in following sections, the quantification and comparison between NO_x uptake and the mechanisms of nitrite/nitrate formation in CAC samples are carried out on granular samples.

3.3.2. NO_x uptake by unmodified CAC

Fig. 7 summarizes the measured N mass, as NO_2^- and NO_3^-, in the NO_x-exposed granular samples. As expected, the samples without NO_x exposure (CAC and CAC5T) show no detectable N, as either NO_2^- or NO_3^-. However, similar N mass as both NO_2^- and NO_3^- were detected in the unmodified CAC samples after NO_x exposure (CAC-N and CAC-NV), regardless of the presence of UV light, and the results are expected due to the absence of TiO_2 in the unmodified CAC samples. The N mass is approximately 6.50 mg kg^{-1} for NO_2^- and 9.40 mg kg^{-1} for NO_3^-. Therefore, this study for the first time quantifies the intrinsic NO_x binding capability of CAC-based cementitious materials, even in the absence of photocatalysts.

The measured N mass of TiO_2-modified CAC samples that are exposed to NO_x (CAC5T-N) is approximately 8.60 mg kg^{-1} for NO_2^- and 11.20 mg kg^{-1} for NO_3^-. Compared to unmodified CAC samples (CAC-N), the total NO_x uptake is increased by 25%, which is similar to the increase of SSA measured in Section 3.1. The result confirms that the increased SSA induced by the inclusion of TiO_2 nanoparticles promotes the surface-related heterogeneous reactions in CAC samples [6,17]. The detection of NO_2^- and NO_3^- ions indicates that these ions produced by the heterogeneous reactions are likely to be physically adsorbed by the hydrated cementitious phases in CAC samples and susceptible to water-based wet chemical extraction [6]. According to Fig. 7, the nitrite-to-nitrate concentration ratio is approximately 1:1.3, suggesting that the heterogeneous reactions converted NO_x more to nitrate than to nitrite by 30% in CAC systems. This discovery is also supported by the work from Pérez-nicolás et al. [30], where they observed that CAC-based samples show a higher NO_2 adsorption than NO, which leads to a higher photo-oxidation of NO_2. The product of this photo-oxidation is nitrate, which is considered a better corrosion inhibitor compared to nitrite when incorporated in cement-based materials [22,47].

3.3.3. NO_x uptake by TiO_2-modified CAC

From Section 3.3.1, the NO_x uptake (m_N) of TiO_2-modified CAC sample (CAC5T) through photocatalytic reactions is approximately 28.4 mg kg^{-1}. If this NO_x binding is transient, such as physically adsorbed by the hydrated cementitious phases as in unmodified CAC, m_N should be equivalent to the summation of photocatalytic converted NO_2^- (m_N') and NO_3^- (m_N''). The m_N' and m_N'' then can be determined by their differences between the samples that are only exposed to NO_x (CAC5T-N) and those that are exposed to both NO_x and UV-light (CAC5T-NV) [6]. However, Fig. 7 shows similar N masses, as NO_2^- and NO_3^-, in both CAC5T-N and CAC5T-NV samples, making the m_N' and m_N'' essentially zero. Therefore, the $m_N \neq m_N' + m_N''$, suggesting a portion of NO_x uptake is chemically bound with TiO_2-modified CAC samples. The mechanisms of how NO_x is chemically bound in CAC samples will be described in detail in Section 3.4.1.

The total NO_x uptake of TiO_2-modified CAC should be determined by separating the contributions from the photocatalytic reactions (m_{N_1} = 28.4 mg kg^{-1}) and the surface-related heterogeneous reactions (m_{N_2} = 20.5 mg kg^{-1}) since both reactions occur intrinsically in the materials. As a result, the total NO_x uptake is determined by $m_N = m_{N\_2} + m_{N\_2}$=48.9 mg kg^{-1}, showing that 58% of the NO_x is chemically bound within the material. The determination of NO_x uptake through photocatalytic reactions, which has been commonly used to determine total NO_x uptake capacity of OPC samples [8,16,48], underestimates the capacity of TiO_2-modified CAC by almost half by neglecting the material's intrinsic NO_x uptake capacity. Therefore, the measurement of NO_x uptake for TiO_2-modified CAC should include the contributions from both photocatalytic and surface-related heterogeneous reactions.

3.4. Comparison between NO_x sequestration in CAC- and OPC-based materials

3.4.1. Mechanism and capacity of NO_x uptake

As discussed in the introduction, the intrinsic NO_x binding capability of cementitious materials have been observed recently. Three mechanisms for NO_x binding have been proposed after the oxidation of NO_x into NO_2^- and NO_3^- through photocatalytic and surface-related heterogeneous reactions [6,16,17,30,49]: I) the adsorption of NO_2^- and NO_3^- on the surface of cement hydrates such as C-S-H, II) the reaction of NO_2^- and NO_3^- with hydroxyl ions in the alkaline pore solution, and III) substitution of NO_2^- and NO_3^- into aluminum-bearing hydrated phases. Since differences in hydration products and microstructural properties between CAC- and OPC-based materials could affect their binding capacity and mechanisms, this section provides a summary of the characteristics of CAC-based samples that could contribute to their NO_x uptake, as compared to the previously examined OPC-based samples [6]. The goal with this discussion is to better understand and quantify the differences in NO_x sequestration between CAC and OPC, considering the three mechanisms noted above.

I. For unmodified cementitious samples, the intrinsic NO_x uptake is induced by the surface-related heterogeneous reactions [7,16], and a higher surface area can facilitate greater reactions and provide more surface area for the adsorption of N-species [6,7,16]. From the previous study for unmodified OPC samples, which was under the same sample preparation (e.g., water-to-solid ratio and TiO_2 dosage) and test conditions as this study [6], the total NO_x uptake (the summation of NO_2^- and NO_3^-) was found to be approximately 8.50 mg kg^{-1}. According to Section 3.3.2, the total NO_x uptake of unmodified CAC samples is 15.90 mg kg^{-1}, an increase by 85% compared to OPC samples. Since the heterogeneous reactions are related to the material's microstructural features, the higher NO_x uptake can be attributed to the larger surface area of CAC samples prepared in this study. The SSA is approximately 10.20 m^2 g^{-1} for OPC [6] and 16.70 m^2 g^{-1} for CAC (Section 3.1). Since the granular OPC and CAC samples have different SSAs, the total intrinsic NO_x uptakes for both materials are further normalized by their respective SSA in this section for the sake of comparison. The surface area-normalized NO_x uptake is estimated to be approximately 8.3 × 10^2 mg mm^{-2} for OPC and 9.5 × 10^2 mg mm^{-2} for CAC. The higher

surface area-normalized NO_x uptake of CAC samples suggests other mechanisms, in addition to surface area, could also play a role in the NO_x uptake.

II. The N-species can react with the hydroxyls (OH^-) presented in the cementitious material [17,18], but CAC typically has a lower pH than OPC [36]. The pH of the hydrated CAC sample was measured at 12.6 [50] and is slightly lower than the OPC sample, which was measured at 13.2 [50]. However, based on the porosity and pH of the hydrated CAC, Alapati [50] has shown that the concentration of OH^- in the hydrated CAC is approximately 0.01 mmol g^{-1} of solid (or 170 mg kg^{-1}). This concentration is >10 times greater than that of the converted N-species, implying there is ample OH^- to react with the N-species exists in CAC. Therefore, the reactions between OH^- and N-species in this CAC-based cementitious environment should be similar to OPC, despite the lower pH of CAC.

III. Section 3.3.3 has shown that the photocatalytic reactions (m_N) are not equal to the summation of photocatalytic converted NO_2^- (m_N') and NO_3^- (m_N''), i.e., $m_N \neq m_N' + m_N''$ for TiO_2-modified CAC samples (CAC5T). However, our previous study [6] has quantified that the $m_N = m_N' + m_N''$ for TiO_2-modified OPC samples. This discrepancy between CAC and OPC can be attributed to the differences in their hydration products (refer to Section 3.1 for the hydrated CAC phases); CAC forms significantly more aluminum-bearing hydrated phases compared to OPC [51,52]. Therefore, this imbalance between the NO_x uptake and converted NO_2^- and NO_3^- should be related to the interactions of converted N-species with these phases.

Studies [19,20] have suggested that the converted NO_2^- and NO_3^- could chemically substitute the interlayer sulfate (SO_4^{2-}) in AFm phases through an anion exchange process. Thermodynamically, it is understood that these anions have a binding preference within AFm phases, with a preference for $NO_3^- > NO_2^- > SO_4^{2-} > OH^-$ [53]. The XRD pattern for the AFm-SO_4 phase that is exposed to NO_x, as shown in Fig. 8, shows a formation of new peaks at 2θ of 9.5° and 15.1° According to Balonis et al. [20], these two peaks respresent AFm-NO_2/NO_3. Therefore, this study for the first time has experimentally demonstrated the formation of AFm-NO_2/NO_3 in a solid-gas reaction through the aforementioned anion exchange process. This anion exchange process could also occur in C_2AH_8 phase, which is one of the major phases in hydrated CAC (Fig. 2), since it is structured similarly to the AFm-SO_4 [36].

In practice, because C_2AH_8 is a metastable phase in CAC and can be converted to more stable phases of AH_3 and C_3AH_6 [42], the conversion of this phase may require control for CAC to be used effectively for NO_x sequestration. Recently, Alapati [50] has demonstrated that carbonation and internal curing could be used to preferentially form C_2AH_8 and in turn maximize the chemically bound NO_x in CAC-based cementitious materials. Further studies, which examine the NO_x binding in other CAC phases such as AH_3, C_3AH_6, and C_2AH_8, are needed to understand the stability of nitrite or nitrate substituted aluminum-bearing phases in CAC over time.

3.4.2. *Sustainability and durability*

Based on the discussion in Part III of Section 3.4.1, this study has shown that these chemically bound NO_2^- and NO_3^- in CAC samples are more resistant to being released by water-based extraction. As discussed in the introduction, release of previously bound N-species back into the environment from OPC-based materials or other substrates remains a concern in developing sequestration materials for sustainability. Therefore, because CAC-based materials have demonstrated a more permanent binding with these ions than OPC-based materials, the use of CAC could be preferred for sequestration applications.

It has been proposed that NO_2^- and NO_3^--containing compounds in cement-based materials can be used at the steel interface to improve the corrosion resistance of steel-reinforced concrete [22,47]. Falzone et al. [22] have demonstrated that chlorides can be fixed in the AFm phases through the aforementioned anion exchange process (Section 3.4.1 and [53]) due to their more favorable binding preference than NO_2^- and NO_3^-. Since chloride-induced steel corrosion is a leading cause of OPC-based concrete infrastructure deterioration, this study has demonstrated that CAC-based infrastructure, which contains TiO_2 photocatalysts, could offer an additional pathway to enhance the inhibition of such corrosion and prolong its service life. In addition, the greater capacity for non-transient chemical NO_x sequestration in CAC is viewed as advantageous over OPC, with regard to enhanced corrosion resistance through increased nitrate and nitrite concentrations in the pore solution.

4. Conclusion and future study

Two sample geometries were prepared to examine the NO_x sequestration performance for both unmodified and TiO_2-modified calcium aluminate cementitious (CAC) materials. The long-term NO_x degradation of TiO_2-modifed CAC was examined using plate samples under a

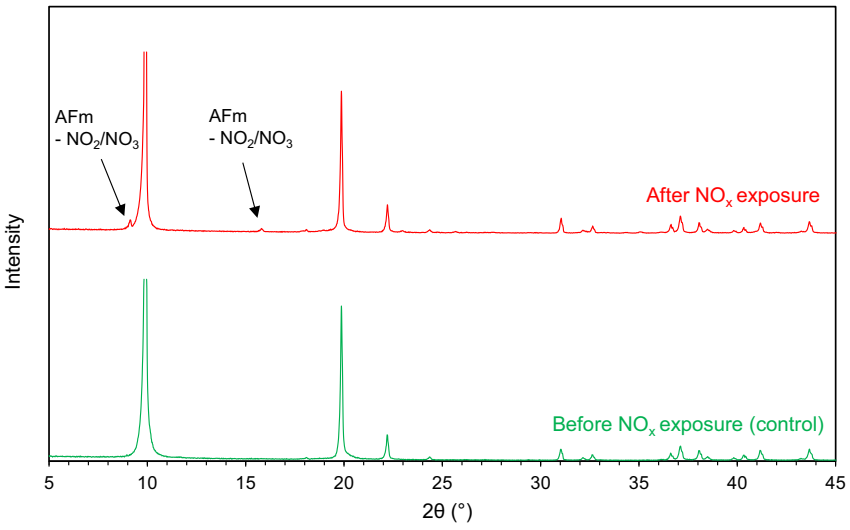

Fig. 8. Two new peaks at 2θ of 9.5° and 15.1° were observed in the XRD patterns of AFm-SO_4 phases before (control) and after NO_x exposure, indicating the formation of AFm- NO_2/NO_3 phases.

multi-cycle test. Granular samples were used to quantify NO_x uptake and explore NO_x binding mechanisms. A combined method of water-based chemical extraction, UV–vis spectrophotometry, and ion chromatography was used to quantify N-species that are bound with hydrated cementitious phases. The effects of composition and microstructural properties on NO_x uptake were examined and a comparison of NO_x uptake between OPC- and CAC-based materials was made. Key conclusions include:

1. The photocatalytic efficiency, η_{NOx}, decreased with increased exposure time and test cycles (from 53% in the first cycle to 40% in the third cycle), implying that the NO_x uptake could reach a limit over time if no surface treatment (e.g., washing) is performed. This decreasing trend also affected the NO_x degradation capacity, which decreased from 800 mmol m^{-2} in the first cycle to 710 mmol m^{-2} in the third cycle. It was also observed that a small fraction of NO_x binding with CAC samples was transient. These effects should be taken into consideration when estimating a material's photocatalytic performance.
2. Similar NO_x uptake was measured in unmodified CAC samples (CAC-N and CAC-NV) regardless of the UV light exposure, demonstrating the material's intrinsic NO_x sequestration capability even in the absence of photocatalysts. The NO_x uptake increased by 25% in TiO_2-modifed CAC that was only exposed to NO_x (CAC5T-N). This increase should be attributed to the increased surface area, which is induced by the inclusion of TiO_2 nanoparticles. The nitrite-to-nitrate concentration ratio was approximately 1:1.3, suggesting that the heterogeneous reactions in CAC systems favor NO_x conversion to nitrate over nitrite.
3. For TiO_2-modified CAC that was exposed to both NO_x and UV light (CAC5T-NV), the photocatalytically-converted nitrite and nitrate cannot be directly measured by water-based chemical extraction, indicating these ions are chemically bound within the CAC materials and resist releasing back into the environment via dissolution. Therefore, the total NO_x uptake of CAC5T-NV can only be determined by separating the contributions from the photocatalytic and surface-related heterogeneous reactions, both of which occur intrinsically in the hydrated CAC materials. Since these chemically bound ions are more resistant to being released back into the environment, the use of CAC can help mitigate the environmental concerns in developing NO_x sequestration materials.
4. The main difference between OPC- and CAC-based materials, in terms of NO_x sequestration, is that the NO_x uptake in OPC through photocatalytic reactions is equal to the summation of photocatalytic converted NO_2^- and NO_3^-, while such balance cannot be detected in CAC. This discrepancy is attributed to the differences in their hydration products, where CAC has significantly higher aluminum content and tends to form more aluminum-bearing hydrated phases compared to OPC. The examination of mineralogical change of synthetic AFm-SO_4 phase before and after its exposure to NO_x has shown the converted NO_2^- and NO_3^- could chemically substitute the interlayer anions through an anion exchange process. These chemically bonded N-species could then enhance the durability of CAC-based concrete infrastructure compared to the OPC-based ones, since NO_2^-- and NO_3^--containing compounds can be used at the steel interface to improve the corrosion resistance of steel-reinforced concrete and, in turn, improve the material's durability.

Based on the findings from this study, future research to improve our understanding of NO_x sequestration in cementitious materials could consider the impact of surface treatment such as washing on the overall photocatalytic efficiency, the interaction of NO_2^- and NO_3^- with other aluminum-bearing phases in CAC-based materials, and NO_x uptake in other aluminum-rich binders such as geopolymers.

CRediT authorship contribution statement

Qingxu Jin: Conceptualization, Investigation, Methodology, Validation, Formal analysis, Data curation, Visualization, Project administration, Writing - Original draft, Writing - Review & editing
Sarah L. Hordern: Investigation, Data curation, Formal analysis, Writing - Review & editing
Yuanzhi Tang: Methodology, Resources, Writing - Review & editing
Kimberly E. Kurtis: Conceptualization, Resources, Project administration, Writing - Review & editing, Supervision, Funding acquisition.

Declaration of competing interest

None.

Acknowledgements

The authors gratefully acknowledge the financial support from the National Science Foundation under Grant No. CMMI-1362843 and EEC-1757579. Any opinions, findings, and conclusions or recommendations expressed in this material are those of the author(s) and do not necessarily reflect the views of the National Science Foundation. The authors would like to thank Paul Stutzman from the National Institute of Standards and Technology for his assistance with electron microscopy, Monday Okoronkwo from the Chemical and Biochemical Engineering Department at Missouri S&T for his preparation of AFm-SO_4 phase, and Hongyan Ma from the Civil, Architectural and Environmental Engineering Department at Missouri S&T for his help with X-ray fluorescence analysis of TiO_2 nanoparticles.

References

[1] J. Riess, Nox: how nitrogen oxides affect the way we live and breathe, US Environmental Protection Agency, Office of Air Quality Planning and Standards, 1998.
[2] D.Q. Tong, L. Lamsal, L. Pan, C. Ding, H. Kim, P. Lee, T. Chai, K.E. Pickering, I. Stajner, Long-term NOx trends over large cities in the United States during the great recession: comparison of satellite retrievals, ground observations, and emission inventories Atmos. Environ. (2015) 70–84, https://doi.org/10.1016/j.atmosenv.2015.01.035.
[3] A. Fujishima, K. Honda, Electrochemical photolysis of water at a semiconductor electrode, Nature 238 (5358) (1972) 37–38, https://doi.org/10.1038/238037a0.
[4] D.E. Macphee, A. Folli, Photocatalytic concretes — The interface between photocatalysis and cement chemistry, Cem. Concr. Res. 85 (2016) 48–54, https://doi.org/10.1016/j.cemconres.2016.03.007.
[5] Q.L. Yu, H.J.H. Brouwers, Indoor air purification using heterogeneous photocatalytic oxidation, Part I: experimental study, Applied Catalysis B : Environmental 92 (3–4) (2009) 454–461, https://doi.org/10.1016/j.apcatb.2009.09.004.
[6] Q. Jin, E.M. Saad, W. Zhang, Y. Tang, K.E. Kurtis, Quantification of NOx uptake in plain and TiO2-doped cementitious materials, Cem. Concr. Res. 122 (2019) 251–256, https://doi.org/10.1016/j.cemconres.2019.05.010.
[7] E. Jimenez-Relinque, J.R. Rodriguez-Garcia, A. Castillo, M. Castellote, Characteristics and efficiency of photocatalytic cementitious materials: Type of binder, roughness and microstructure Cem. Concr. Res. (2015) 124–131, https://doi.org/10.1016/j.cemconres.2015.02.003.
[8] J. Chen, C.S. Poon, Photocatalytic construction and building materials: from fundamentals to applications, Build. Environ. 44 (9) (2009) 1899–1906, https://doi.org/10.1016/j.buildenv.2009.01.002.
[9] Photocatalysts: technologies and global markets: AVM069B. BCC Research. https://www.bccresearch.com/market-research/advanced-materials/photocatalysts-technologies-markets-report.html , 3 December 2019. (n.d.).
[10] Photocatalyst market size worth $ 4.56 billion by 2025|CAGR: 11.5%. https://www.prnewswire.co.uk/news-releases/photocatalyst-market-size-worth–456-billion-by-2025–cagr-115-grand-view-research-inc-668286473.html, 3 December 2019. (n.d.).
[11] Y. Hendrix, A. Lazaro, Q.L. Yu, H.J.H. Brouwers, Titania-silica composites: a review on the photocatalytic activity and synthesis methods, World J. Nano Sci. Eng. 05 (2015) 161–177, https://doi.org/10.4236/wjnse.2015.54018.
[12] A. Pietrzak, J. Adamus, B. Langier, Application of titanium dioxide in cement and concrete technology, Key Engineering Materials 687 (2016) 243–249, https://doi.org/10.4028/www.scientific.net/kem.687.243.
[13] Jin Q., Faraldos M., Bahamonde A., Zaribaf B.H., Kurtis K.E., Titania and silica nanoparticle-modified coatings for cementitious materials ACI Symposium

Publication 2019 97-111. https://www.concrete.org/publications/internationalconcreteabstractsportal.aspx?m=details&id=51720218.
[14] M.M. Ballari, M. Hunger, G. Hüsken, H.J.H. Brouwers, NOx photocatalytic degradation employing concrete pavement containing titanium dioxide, Applied Catalysis B: Environmental 95 (3–4) (2010) 245–254, https://doi.org/10.1016/j.apcatb.2010.01.002.
[15] M.M. Ballari, M. Hunger, G. Hüsken, H.J.H. Brouwers, Modelling and experimental study of the NOx photocatalytic degradation employing concrete pavement with titanium dioxide, Catalysis Today 151 (1–2) (2010) 71–76, https://doi.org/10.1016/j.cattod.2010.03.042.
[16] A.M. Kaja, H.J.H. Brouwers, Q.L. Yu, NOx degradation by photocatalytic mortars: The underlying role of the CH and C-S-H carbonation, Cem. Concr. Res. 125 (2019) 105805, https://doi.org/10.1016/j.cemconres.2019.105805.
[17] V.H. Grassian, Chemical Reactions of Nitrogen Oxides on the Surface of Oxide, Carbonate, Soot, and Mineral Dust Particles: Implications for the Chemical Balance of the Troposphere, J. Phys. Chem. A. 106 (6) (2002) 860–877, https://doi.org/10.1021/jp012139h.
[18] M. Horgnies, I. Dubois-Brugger, E.M. Gartner, NOx de-pollution by hardened concrete and the influence of activated charcoal additions, Cem. Concr. Res. (2012) 1348–1355, https://doi.org/10.1016/j.cemconres.2012.06.007.
[19] G. Falzone, M. Balonis, G. Sant, X-AFm stabilization as a mechanism of bypassing conversion phenomena in calcium aluminate cements, Cem. Concr. Res. 72 (2015) 54–68, https://doi.org/10.1016/j.cemconres.2015.02.022.
[20] M. Balonis, M. Mędala, F.P. Glasser, Influence of calcium nitrate and nitrite on the constitution of AFm and AFt cement hydrates, Adv. Cem. Res. 23 (3) (2011) 129–143, https://doi.org/10.1680/adcr.10.00002.
[21] M. Balonis, F.P. Glasser, Calcium nitrite corrosion inhibitor in portland cement: influence of nitrite on chloride binding and mineralogy, J. Am. Ceram. Soc. 94 (7) (2011) 2230–2241, https://doi.org/10.1111/j.1551-2916.2010.04362.x.
[22] G. Falzone, M. Balonis, D. Bentz, S. Jones, G. Sant, Anion capture and exchange by functional coatings: New routes to mitigate steel corrosion in concrete infrastructure, Cem. Concr. Res. 101 (2017) 82–92, https://doi.org/10.1016/j.cemconres.2017.08.021.
[23] H. Ye, Z. Chen, Influence of nitrate corrosion inhibitors on phase stability of alkali-activated slag against chloride binding and natural carbonation, J. Mater. Civ. Eng. 31 (8) (2019), https://doi.org/10.1061/(asce)mt.1943-5533.0002830, 04019160.
[24] H. Ye, Autogenous formation and smart behaviors of nitrite- and nitrate-intercalated layered double hydroxides (LDHs) in Portland cement-metakaolin-dolomite blends, Cem. Concr. Res. 139 (2021) 106267, https://doi.org/10.1016/j.cemconres.2020.106267.
[25] P. Gundersen, I.K. Schmidt, K. Raulund-Rasmussen, Leaching of nitrate from temperate forests - effects of air pollution and forest management, Environ. Rev. 14 (1) (2006) 1–57, https://doi.org/10.1139/a05-015.
[26] R. Sugrañez, J.I. Álvarez, M. Cruz-Yusta, I. Mármol, J. Morales, J. Vila, L. Sánchez, Enhanced photocatalytic degradation of NOx gases by regulating the microstructure of mortar cement modified with titanium dioxide, Build. Environ. 69 (2013) 55–63, https://doi.org/10.1016/j.buildenv.2013.07.014.
[27] C. Cárdenas, J.I. Tobón, C. García, J. Vila, Functionalized building materials: photocatalytic abatement of NOx by cement pastes blended with TiO2 nanoparticles, Constr. Build. Mater. (2012) 820–825, https://doi.org/10.1016/j.conbuildmat.2012.06.017.
[28] M. Kaneko, I. Okura, Photocatalysis : science and technology, Springer, Berlin, 2002.
[29] B.Y. Lee, K.E. Kurtis, Durability of photocatalytic cement subjected to nitrogen dioxide and wet–dry cycling, Adv. Cem. Res. (2020) 139–147.
[30] M. Pérez-nicolás, J. Balbuena, M. Cruz-yusta, L. Sánchez, I. Navarro-blasco, J. M. Fernández, J.I. Alvarez, Photocatalytic NOx abatement by calcium aluminate cements modified with TiO2: Improved NO2 conversion, Cem. Concr. Res. 70 (2015) 67–76, https://doi.org/10.1016/j.cemconres.2015.01.011.
[31] T. Pyatina, T. Sugama, Acid resistance of calcium aluminate cement–fly ash F blends, Adv. Cem. Res. 28 (7) (2016) 433–457, https://doi.org/10.1680/jadcr.15.00139.
[32] H.A. Khan, A. Castel, M.S.H. Khan, A.H. Mahmood, Durability of calcium aluminate and sulphate resistant Portland cement based mortars in aggressive sewer environment and sulphuric acid, Cem. Concr. Res. 124 (2019) 105852, https://doi.org/10.1016/j.cemconres.2019.105852.
[33] ISO 22197-1:2016Fine ceramics (advanced ceramics, advanced technical ceramics) — Test method for air-purification performance of semiconducting photocatalytic materials — Part 1: Removal of nitric oxide. https://www.iso.org/standard/65416.html.
[34] JIS R 1701-1, Fine Ceramics (Advanced Ceramics, Advanced Technical Ceramics)—Test Method for Air Purification Performance of Photocatalytic Materials—Part 1: Removal of Nitric Oxide, Japanese Standards Association, Tokyo, Japan, 2016, 22 pp.
[35] T. Matschei, B. Lothenbach, F.P. Glasser, The AFm phase in Portland cement, Cem. Concr. Res. 37 (2) (2007) 118–130, https://doi.org/10.1016/j.cemconres.2006.10.010.
[36] C. Gosselin, Microstructural Development of Calcium Aluminate Cement Based Systems With and Without Supplementary Cementitious Materials (PhD Thesis), EPFL, 2009, https://doi.org/10.5075/epfl-thesis-4443.
[37] S. Brunauer, P.H. Emmett, E. Teller, Adsorption of gases in multimolecular layers, J. Am. Chem. Soc. (1938) 309–319, https://doi.org/10.1021/ja01269a023.
[38] I. Odler, The BET-specific surface area of hydrated Portland cement and related materials, Cem. Concr. Res. (2003) 2049–2056, https://doi.org/10.1016/S0008-8846(03)00225-4.
[39] M.C.G. Juenger, H.M. Jennings, The use of nitrogen adsorption to assess the microstructure of cement paste, Cem. Concr. Res. (2001) 883–892, https://doi.org/10.1016/S0008-8846(01)00493-8.
[40] J.W. Bullard, Q. Jin, K.A. Snyder, How do specific surface area and particle size distribution change when granular media dissolve? Chem. Eng. J. 406 (2021) 127098, https://doi.org/10.1016/j.cej.2020.127098.
[41] Q. Jin, L.N. Perry, J.W. Bullard, Temperature dependence of gypsum dissolution rates Cem, Concr. Res. 129 (2020) 105969, https://doi.org/10.1016/j.cemconres.2019.105969.
[42] K. Scrivener, R. Snellings, B. Lothenbach, A practical guide to microstructural analysis of cementitious materials, CRC Press, Taylor & Francis, 2016.
[43] J. Chen, C.S. Poon, Photocatalytic activity of titanium dioxide modified concrete materials - influence of utilizing recycled glass cullets as aggregates, J. Environ. Manage. 90 (11) (2009) 3436–3442, https://doi.org/10.1016/j.jenvman.2009.05.029.
[44] Q. Jin, Fundamental Understanding of NOx Sequestration Capacity and Pathways in Nano-TiO2 Engineered Cementitious Materials (PhD Thesis) Georgia Institute of Technology, 2019.
[45] M.M. Hassan, H. Dylla, L.N. Mohammad, T. Rupnow, Evaluation of the durability of titanium dioxide photocatalyst coating for concrete pavement, Constr. Build. Mater. 24 (8) (2010) 1456–1461, https://doi.org/10.1016/j.conbuildmat.2010.01.009.
[46] J. Chen, C.S. Poon, Photocatalytic cementitious materials: influence of the microstructure of cement paste on photocatalytic pollution degradation, Environ. Sci. Technol. 43 (23) (2009) 8948–8952, https://doi.org/10.1021/es902359s.
[47] M. Büchler, Corrosion inhibitors for reinforced concrete, Corros. Reinf. Concr. Struct. (2005) 190–214, https://doi.org/10.1533/9781845690434.190.
[48] L. Cassar, Photocatalysis of cementitious materials: clean buildings and clean air, MRS Bull. 29 (5) (2004) 328–331, https://doi.org/10.1557/mrs2004.99.
[49] B.Y. Lee, A.R. Jayapalan, M.H. Bergin, K.E. Kurtis, Photocatalytic cement exposed to nitrogen oxides: effect of oxidation and binding, Cem. Concr. Res. 60 (2014) 30–36, https://doi.org/10.1016/j.cemconres.2014.03.003.
[50] P. Alapati, Multiscale Investigation of Alternative Cementitious Material Systems (PhD Thesis) Georgia Institute Technology, 2020.
[51] J. Bizzozero, K.L. Scrivener, Limestone reaction in calcium aluminate cement-calcium sulfate systems, Cem. Concr. Res. 76 (2015) 159–169, https://doi.org/10.1016/j.cemconres.2015.05.019.
[52] K.L. Scrivener, J.L. Cabiron, R. Letourneux, High-performance concretes from calcium aluminate cements, Cem. Concr. Res. 29 (8) (1999) 1215–1223, https://doi.org/10.1016/S0008-8846(99)00103-9.
[53] G. Puerta-Falla, M. Balonis, G. Falzone, M. Bauchy, N. Neithalath, G. Sant, Monovalent ion exchange kinetics of hydrated calcium-alumino layered double hydroxides, Ind. Eng. Chem. Res. 56 (1) (2017) 63–74, https://doi.org/10.1021/acs.iecr.6b03474.